Advanced Structured Materials

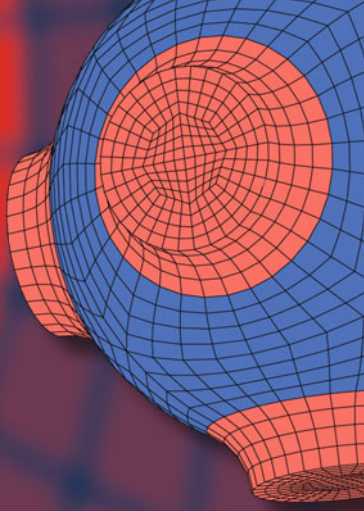

Andreas Öchsner
Holm Altenbach *Editors*

Engineering Design Applications II

Structures, Materials and Processes

Springer

Advanced Structured Materials

Volume 113

Common engineering materials reach in many applications their limits and new developments are required to fulfil increasing demands on engineering materials. The performance of materials can be increased by combining different materials to achieve better properties than a single constituent or by shaping the material or constituents in a specific structure. The interaction between material and structure may arise on different length scales, such as micro-, meso- or macroscale, and offers possible applications in quite diverse fields.

This book series addresses the fundamental relationship between materials and their structure on the overall properties (e.g. mechanical, thermal, chemical or magnetic etc.) and applications.

The topics of *Advanced Structured Materials* include but are not limited to

- classical fibre-reinforced composites (e.g. glass, carbon or Aramid reinforced plastics)
- metal matrix composites (MMCs)
- micro porous composites
- micro channel materials
- multilayered materials
- cellular materials (e.g., metallic or polymer foams, sponges, hollow sphere structures)
- porous materials
- truss structures
- nanocomposite materials
- biomaterials
- nanoporous metals
- concrete
- coated materials
- smart materials

Advanced Structured Materials is indexed in Google Scholar and Scopus.

More information about this series at http://www.springer.com/series/8611

Andreas Öchsner · Holm Altenbach
Editors

Engineering Design Applications II

Structures, Materials and Processes

Springer

Editors
Andreas Öchsner
Faculty of Mechanical Engineering
Esslingen University of Applied Sciences
Esslingen, Baden-Württemberg, Germany

Holm Altenbach
Lehrstuhl für Technische Mechanik
Institut für Mechanik
Faculty of Mechanical Engineering
Otto-von-Guericke-Universität Magdeburg
Magdeburg, Sachsen-Anhalt, Germany

ISSN 1869-8433 ISSN 1869-8441 (electronic)
Advanced Structured Materials
ISBN 978-3-030-20800-4 ISBN 978-3-030-20801-1 (eBook)
https://doi.org/10.1007/978-3-030-20801-1

This Springer imprint is published by the registered company Springer Nature Switzerland AG
The registered company address is: Gewerbestrasse 11, 6330 Cham, Switzerland

Preface

Different engineering disciplines such as mechanical, materials, computer and process engineering provide the foundation for the design and development of improved structures, materials and processes. The modern design cycle is characterized by an interaction of different disciplines and a strong shift to computer-based approaches where only a few experiments are performed for verification purposes. A major driver for this development is the increased demand for cost reduction, which is also connected to environmental demands. In the transportation industry (e.g. automotive or aerospace), this is connected with the demand for higher fuel efficiency, which is related to the operational costs and the lower harm for the environment. One way to fulfil such requirements is lighter structures and/or improved processes for energy conversion. Another emerging area is the interaction of classical engineering with the health and medical sector. This volume gives an update on recent developments in the mentioned areas of modern engineering design application.

We would like to express our sincere appreciation to the representatives of Springer, who made this volume possible.

Esslingen, Germany — Prof. Dr.-Ing. Andreas Öchsner, D.Sc.
andreas.oechsner@gmail.com

Magdeburg, Germany — Prof. Dr.-Ing. habil. Dr. h. c. mult. Holm Altenbach
holm.altenbach@ovgu.de

Contents

Investigation of the Damage Behavior of Polyurethane in Stress Relaxation Experiments and Estimation of the Stress-at-Break σ_b with a Failure Envelope

Selina Neuhaus, Henning Seibert and Stefan Diebels

Abstract In stress relaxation experiments the investigated polyurethane exhibits an unexpected, but repeatable failure during the relaxation period. Images, taken by a camera and a high speed camera, displayed crack initiation several minutes before rupture occurred. The crack growth rate then accelerates and leads to failure rapidly. The present investigation indicates different methods for analyzing the damage evolution with focus on the appearance of damage at low strains, accumulation of damage processes at higher strains, the influence of time on damage evolution and the identification of recovery phenomena during unloading and in the unloaded state. The results show that not only long times at high strains but also the loading history, especially loading and unloading processes, accelerate damage evolution. In a preliminary study the characterization of the ultimate tensile properties by a failure envelope appears to provide an adequate method for estimating the stress-at-break σ_b and the time-to-break t_b in stress relaxation experiments.

Keywords Digital image correlation · Crack initiation · Crack growth · Damage evolution · Predeformation · Failure envelope

1 Introduction

Stress relaxation experiments are usually used to characterize the viscoelastic behavior of polymers [1–4]. During the relaxation period a stress decay due to the viscoelasticity is measurable. In general, damage rises with increasing stress [5]. In spite of the decrease of stress in stress relaxation experiments, the investigated polyurethane ruptures. Friedrich [6] also observed this damage behavior on an ethylene-propylene-diene monomer rubber. Especially in technical use of these materials such an unexpected failure has to be avoided. For this purpose, it is important to characterize the fracture process and to study the damage evolution as well as its dependencies from testing conditions. Friedrich [6] already showed, that the time-to-break during

S. Neuhaus (✉) · H. Seibert · S. Diebels
Applied Mechanics, Saarland University, Campus A4.2, 66123 Saarbrücken, Germany
e-mail: selina.neuhaus@uni-saarland.de

A. Öchsner and H. Altenbach (eds.), *Engineering Design Applications II*,
Advanced Structured Materials 113, https://doi.org/10.1007/978-3-030-20801-1_1

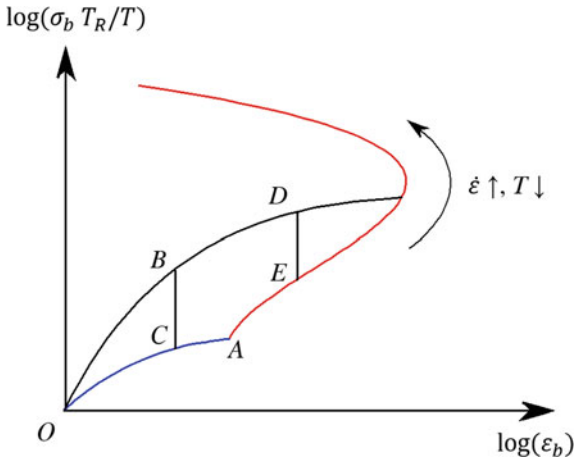

Fig. 1 Schematic representation of the failure envelope which connects rupture points from different tensile tests, used to estimate rupture in stress relaxation experiments

stress relaxation depends on the temperature, the strain rate and the maximal applied strain. In his experiments damage seemed to become minimal at a specific intermediate strain rate. Furthermore, he defined an upper threshold strain value ε_{oG} at which samples already break during loading, and a lower threshold strain value ε_{uG} , at which the specimens do not fail over the entire testing period.

Smith and Stedry [7] also observed rupture during the stress relaxation of a styrene-butadiene rubber. They developed a method to use the stress-strain data from tensile tests to estimate the stress-at-break σ_b, at which rupture occurs in stress relaxation and creep experiments. The ultimate properties are considered in terms of stress-strain curves to rupture measured at various temperatures and strain rates. In a diagram these rupture points $(\varepsilon_b|\sigma_b)$ are connected and build the so-called failure envelope (see Fig. 1). The plot of $\log(\sigma_b\, T_R/T)$ versus the logarithm of the strain-at-break ε_b, where T is the testing temperature and T_R is an arbitrary reference temperature, considers that the elastic retractive force in a specimen at a fixed extension ratio increases in direct proportion to the absolute temperature [8]. Provided time-temperature superposition is applicable, the failure envelope is independent of temperature, strain rate and testing method [7–9]. In Fig. 1 the curve $\overline{OA}$ represents stress-strain values under nearly equilibrium conditions in the absence of viscous effects. If a specimen is stretched along curve $\overline{OB}$ and the strain is held constant, stress will relax until it reaches C on the equilibrium stress-strain curve. But if the sample is elongated along curve $\overline{OD}$ and thereafter the strain is held constant, stress decreases and the specimen breaks by intersecting the failure envelope at E. Indeed, rupture can also occur along the equilibrium curve. Even though there is no viscous relaxation, the ultimate properties of tensile tests with nearly equilibrium conditions vary considerably with temperature and strain rate. Hence, A is not a sharp corner but a fluent transition from the equilibrium curve to the failure envelope [8].

2 Experimental

First the sample preparation, the sample geometry and the testing device are explained. Then the different experiments and the results are presented. In conventional stress relaxation experiments the relaxation behavior and the fracture process are investigated. Afterwards, different modifications of the stress relaxation experiment are outlined to study the time and loading history dependence of the damage evolution. At the end in a preliminary study the method of Smith and Stedry [7] appears to be an adequate possibility to estimate the stress-at-break σ_b in stress relaxation experiments.

2.1 Material and Apparatus

The investigated material is a cross-linked polyurethane. The monomer components used to prepare the samples were supplied by the manufacturer Covestro AG. A mixture of polyether-based diol (Desmophen® 3600Z) and polyether-based triol (Baygal® K 55) is used as the resin component with 90% of the hydroxyl groups of the diol and 10% of the triol. Hence, the resulting polyurethane is called PU90/10. The crosslinking agent is a diphenylmethane diisocyanate isomer mixture (Desmodur® VP.PU 1806) that is stoichiometrically mixed with the resin. To avoid undesirable reactions with water from the air, the total sample preparation was performed in a glove box. The polyurethane was then injected into individual grooves milled into a Teflon mold and allowed to cure a week at room temperature in dried air and afterwards a week at 60 °C in dried air. After this curing time the samples were removed from the Teflon mold. The thereby introduced internal stresses were reduced by a heat treatment at 60 °C for 20 min. The samples were then stored in a dry box.

The material was tested displacement-controlled with a uniaxial testing device at 30 °C in a heat chamber. In order to obtain the desired uniform temperature, the samples were preheated in the unstrained state for 15 min before they were elongated. In previous tensile tests the relation between the applied machine displacement and the strain in loading direction ε_{xx} and in cross direction ε_{yy} was determined via digital image correlation DIC. Hence, it was possible to execute the stress relaxation experiments without DIC using the calibration curves. The Cauchy-stress was then calculated by the ratio of the measured load F and the current cross-section ($(1 + \varepsilon_{yy})^2\, bd$) with an initial sample width b and an initial sample thickness d

$$\sigma = \frac{F}{(1 + \varepsilon_{yy})^2} bd. \tag{2.1}$$

The results of the DIC also showed the compressible stress-strain behavior of PU90/10. The Poisson's ratio was determined to be approximately 0.39. A special waisted sample geometry (see Fig. 2) realizes a smallest cross-section area in the

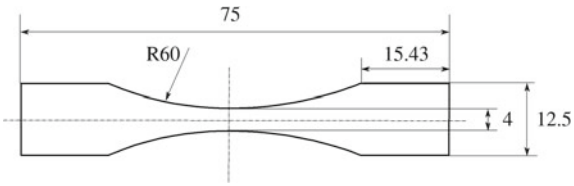

Fig. 2 Sample geometry with a sample thickness of 2 mm

center of the specimen with highest stresses and generates a replicable predetermined breaking point.

2.2 Experiments and Results

2.2.1 Conventional Stress Relaxation Experiments

Conventional stress relaxation experiments to rupture were carried out to get an overview of the relaxation behavior and the fracture process. Ten experiments provided a mean value of the time-to-break t_b of about 1040.5 s with a broad scattering (see Fig. 6) and a standard deviation of 887.1 s. t_b is the elapsed time from the beginning of the stress relaxation period until rupture occurs. All tests were conducted at 30 °C and with a rate of extension of 0.1 mm/s to a machine displacement of 50 mm. The maximal axial strain reaches about 200%. The elongation was held constant until the specimens broke. With these parameters PU90/10 shows a significant viscoelastic behavior in combination with a comparatively short time-to-break.

A DIC-picture (see Fig. 3) shows that the deformation is homogeneous in the middle of the sample. There is no strain concentration at one side, so the testing machine was axial well aligned. In one extra test, images were taken using a camera during the loading and the relaxation period to study the crack initiation and growth. The last seconds before rupture was recorded with a high speed camera to investigate the fracture process. Figure 4 shows the first frame of the high speed camera which displays the cracked sample.

In this investigation the crack appears during loading (see star symbol in Fig. 5) at 43 mm machine displacement. In some subsequent tests cracks just became visible during stress relaxation. In all cases the incipient crack appears long time before failure. In some samples the crack did not appear in the center of the sample which indicates pores inside the specimen. The results of these tests were omitted. The crack length in the pictures of both the camera (see square symbols in Fig. 5) and the high speed camera (see triangle symbols in Fig. 5) was measured with the software National Instruments Vision Assistant 2015. At the beginning of the relaxation period the crack grows barely. Predominantly after a longer time of about 3830 s crack growth increases markedly and the crack tip sharpens while necking in the fracture

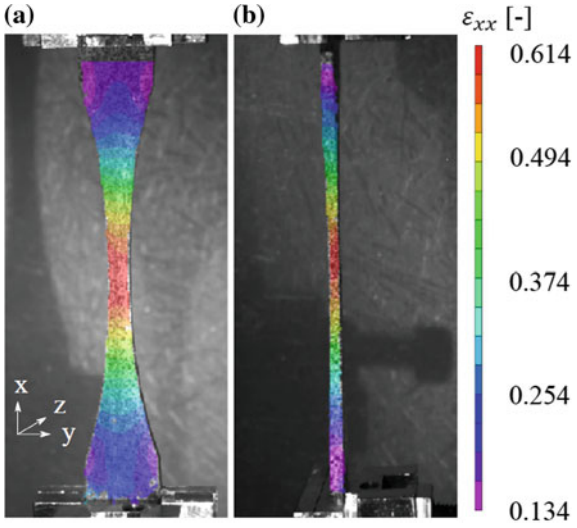

Fig. 3 DIC of a sample in (**a**) front view and (**b**) side view and the determined strain ε_{xx} in tensile direction

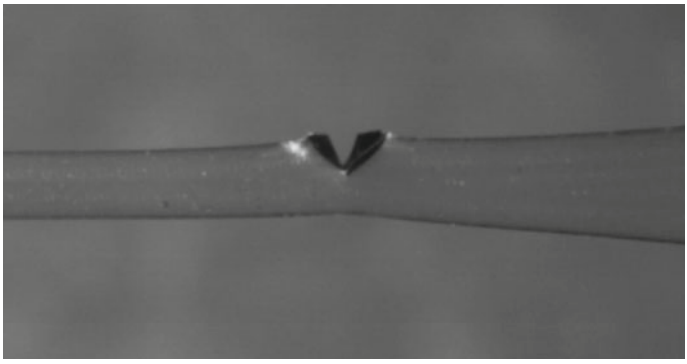

Fig. 4 Cracked sample 2.876 s before rupture occurred, picture taken with a high speed camera with 3000 frames per second

region and bending towards the crack arise. Total rupture occurred after 4995 s testing time.

Sometimes samples slipped slightly out of the clamps during testing. Hence, the effective applied strain and the achieved stress was less than expected. This also affects the strain rate. The local stress-strain behavior appeared to be independent of the slippage, so the reliability and the reproducibility of the results are still guaranteed. After every experiment the maximal stress σ_{max} at the beginning of the relaxation period when the maximum axial displacement is reached and the stress-at-break σ_{min} as the mean value of the last 5 recorded measurements before rupture were

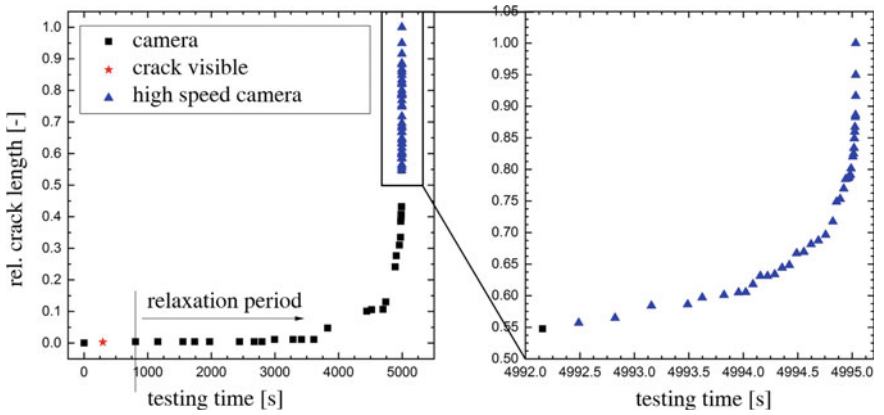

Fig. 5 Increasing crack length related to the initial sample thickness in a stress relaxation experiment

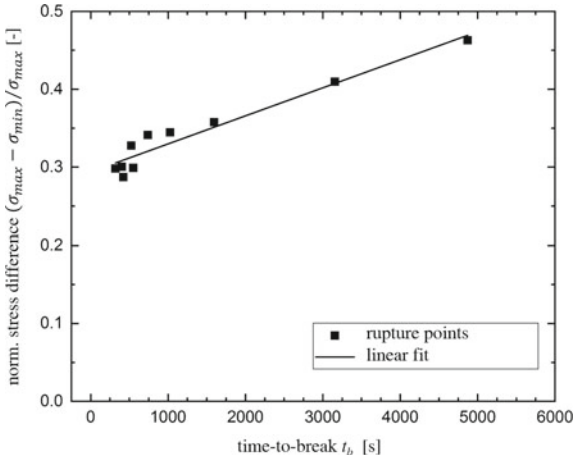

Fig. 6 Normalized stress difference of ten conventional stress relaxation experiments to rupture

determined. The difference between σ_{max} and σ_{min} was calculated to compare the stress decays of different tests, to characterize the intrinsic material behavior and to quantify the sustained load. However, the less the maximal stress because of slippage of the sample out of the clamps, the slower the initial stress decay in the relaxation period [10, 11]. To reduce this effect, the calculated stress difference was divided by the maximal stress. The dependence of the so obtained normalized stress differences of the ten conventional stress relaxation experiments on the time-to-break t_b can be described by a straight line (see Fig. 6). This relation can be used as a failure criterion in a damage mechanics model.

2.2.2 Discontinuous Relaxation Experiments

To investigate the dependency of the damage evolution on the test duration and the overall time at high strains, in the second test series relaxation experiments were interrupted by several unloading processes and subsequent waiting times, at which the sample remains unstretched. After these waiting times the sample was reloaded up to a machine displacement of 50 mm and again stress relaxation with the same holding time than before was conducted. A waiting time of one day between each cycle of loading, stress relaxation and unloading was chosen for fifteen samples. Fifteen further samples were stored two weeks before the next cycle was conducted. At least, the cycles were performed one after another without waiting time (0 s) for fifteen specimens as well. The maximal waiting time of two weeks after one cycle of loading, stress relaxation and unloading was chosen because the specimen's length regains then its initial value. Hence, time-dependent internal stresses are mostly relieved after two weeks and the PU appears to deform viscoelastically. Therefore, the plastic part of deformation can be neglected. These experiments compared to those without a waiting time between the single cycles also allow to find out if there are recovery processes that reduce or at least retard damage. In the discontinuous relaxation experiments the samples with one day or two weeks of waiting time performed maximal five cycles provided they do not break before. However, those without waiting time were tested until rupture occurred also if more than five cycles were necessary.

The holding time, that defines how long the sample is exposed to the maximal strain, is another parameter, which was varied between 300, 500 and 800 s. Hence, the stress relaxation of five of the fifteen samples with a waiting time of one day (or two weeks or 0 s) was 300 s in every cycle. One half of the remaining ten specimens was exposed to 500 s and the other half to 800 s stress relaxation in each cycle. The mean time-to-break of 1040.5 s of the ten conventional relaxation experiments is the reason for this choice of holding times. Assuming that the mean time-to-break of conventional experiments is comparable to the overall time at maximal strain of all cycles of an interrupted relaxation experiment, rupture is expected to occur in the fourth cycle if the holding time in each cycle is 300 s. Analogously, with a holding time of 500 s or 800 s the sample is anticipated to break in the third or the second cycle. 300 s is the smallest holding time, because in conventional relaxation experiments no specimen failed in this time.

Besides, five other samples were tested in a cyclic test (without waiting time and without holding time) with a mean displacement of 25 mm and a maximal displacement of 50 mm. So, a total number of 50 discontinuous relaxation experiments were performed. Combining the different holding times with the mentioned values for the waiting times, ten interrupted relaxation experiments, including the cyclic tests, can be distinguished, which were each repeated with five samples. Figure 7 illustrates exemplary the five experiments with two weeks waiting time and 800 s holding time. The tests were carried out in a displacement-controlled manner, which cause small compressive stresses after unloading.

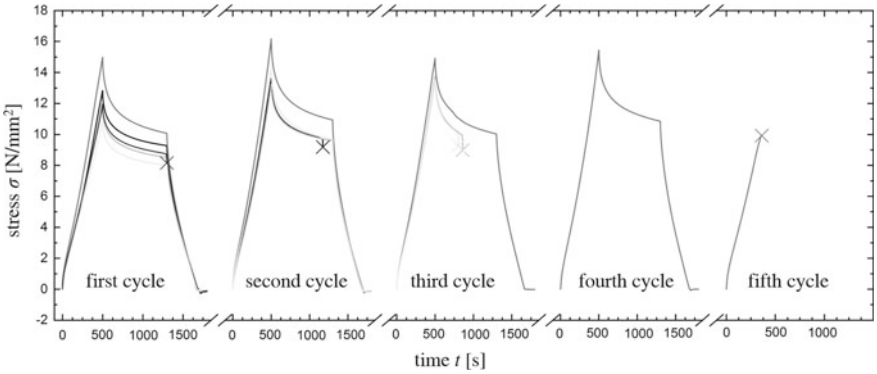

Fig. 7 Stress-time-diagrams of the five discontinuous relaxation experiments with two weeks waiting time (marked with breaks //) and 800 s holding time: crosses mark the rupture points, different gray scales represent distinct samples

Especially in the case of the sample with the highest maximal stress in every cycle an increase of stress in the second cycle compared to the first cycle can be observed. This effect just emerges in the experiments with a waiting time of one day or two weeks because in these tests the specimens were removed from the clamps and again stored in the dry box between the single cycles. When clamping the sample once again to conduct the next cycle, the preload and the clamping is not 100% identical to those in the previous cycle. Therefore, the test starting conditions differ in a series of discontinuous relaxation test. Also the measurement inaccuracy due to slippage is more pronounced, because it varies not only from sample to sample but also from cycle to cycle. The better the clamping, the less the slippage of the sample and the higher the achieved stress. The discontinuous relaxation experiments with waiting times of one day or two weeks provide comparable results. So, the relaxation processes between one day and two weeks appear not to significantly influence the results.

The assumption of damage being reduced or retarded by recovery effects is not confirmed. On the contrary, the samples in tests without waiting time tend to withstand the maximal loading for longer. A conceivable reason may be the fact, that between the cycles in these tests, the samples were not removed from the clamps. Hence, the results of the discontinuous relaxation experiments without waiting time always show a decrease of the maximal stress from cycle to cycle due to the viscoelastic behavior of the polyurethane. In the interrupted relaxation experiments with waiting times viscoelasticity leads to relaxation processes which relieve time-dependent stresses. Thus, in the next cycle the maximal stress is higher. But with increasing maximal stress, the lifetime of the specimen tends to decrease. Besides, the normalized stress difference is higher.

In consequence of the influence of the viscoelasticity, the clamping and the slippage on the results, together with the broad scattering of the time-to-break, comparability between experiments with and without waiting time is reduced. On this basis,

it is not possible to get information about the existence of recovery effects during the waiting time and their influence on damage evolution.

To guarantee better comparability of the results of the experiments with and without waiting time, in further investigations samples could also be removed from the clamps in the latter case. On the other hand, the first cycle of these experiments without waiting time can be conducted as shown above and its maximal stress can be preset as the beginning of the stress relaxation in all further cycles. Then DIC will be necessary with the maximal strain differing from cycle to cycle.

In the discontinuous stress relaxation experiments the PU90/10 specimen tended to sustain more cycles before rupture than expected regarding the mean time-to-break in conventional relaxation tests. This is shown by three diagrams in Fig. 8. The ordinate displays the number of cycles within which the begin of the relaxation period was reached before failure occurred. So, the breaking point of a sample which broke during loading in the third cycle is plotted at a number of cycles of 2. The gray scale illustrates the relative number of broken samples at the considered breaking point. This is used as an estimation for the probability of fracture with increasing time. Since each of the ten different discontinuous relaxation experiments was repeated with five samples, a probability of fracture increases from 0.2 to 1 between the first and the fifth breaking point. The abscissa depicts the total testing time including loading, stress relaxation and unloading process of every cycle. The experimental results are divided into three diagrams according to the waiting time.

The fact, that the investigated material sustained more cycles than expected, indicates, that damage depends not only on the endured time at high deformation but also on the loading history, meaning the foregoing loading and unloading paths. Loading and unloading appear to be correlated with damage because samples also break in a cyclic test without waiting time and holding time. Besides, the maximal time-to-break in the cyclic tests is only slightly higher than in discontinuous relaxation experiments with 800 s holding time.

In the tests with waiting times of one day or two weeks, the samples tendentially sustain the least cycles in the experiments with 500 s holding time instead of those with relaxation periods of 800 s, although the percentage of overall time at maximal strain with respect to the total testing time decreases with decreasing holding time. With holding times of 300 s or 500 s the samples also appear to fail earlier than in tests with 800 s. A reduction of the holding time makes the loading and unloading paths all the more significant. Therefore, both the loading history and the overall time at high strains initiate damage processes and lead to failure.

2.2.3 Relaxation Experiments with Preceding Deformation

The light gray curves in Fig. 9 demonstrate the two different kinds of deformation, that were carried out two weeks before a stress relaxation experiment at 50 mm maximal machine displacement to rupture was conducted. On the one hand samples were elongated to 50 mm machine displacement with 0.1 mm/s and immediately unloaded with the same machine rate (see “peak”‘ in Fig. 9(a)). The previous exper-

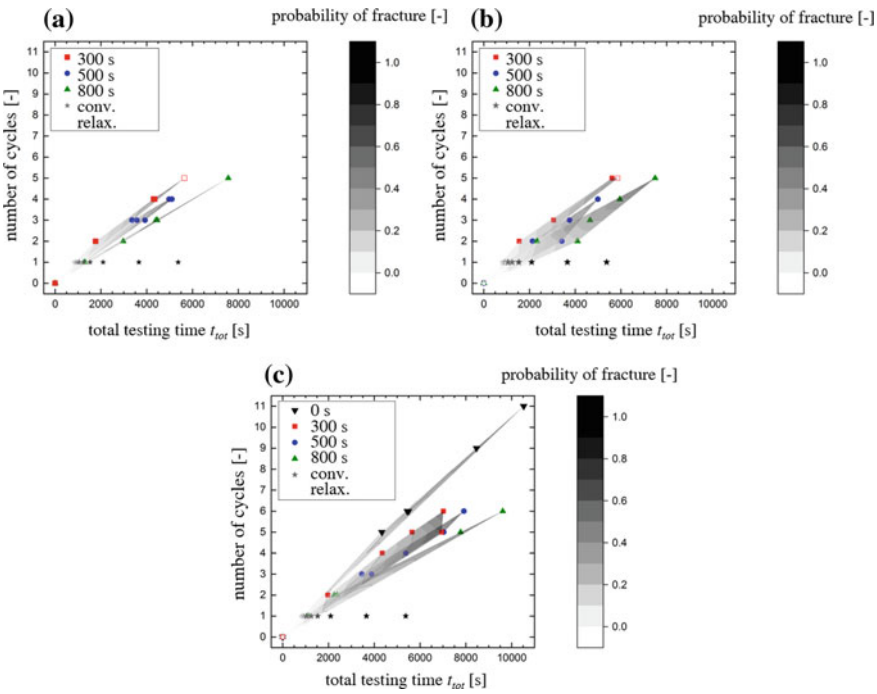

Fig. 8 Probability of fracture depending on the total testing time and the number of sustained cycles split in three diagrams according to the waiting time: (**a**) two weeks, (**b**) one day and (**c**) without waiting time

iments showed that damage depends on time at high strains and loading history. The preceding deformation should clarify, if damage processes already proceed during loading or if they mostly need enough time to form. In the first case damage should be measurable in a following loading process in form of a decrease of the time-to-break of the polyurethane in the relaxation period.

On the other hand, a stress relaxation experiment with a holding time of two hours at 10 mm machine displacement was conducted to see if damage also appears at low strains. 10 mm appeared to be less than the lower threshold strain value ε_{uG} because even after 18 h holding time at 10 mm the sample did not have any visible cracks. To avoid an influence of time-dependent viscoelastic effects on the stress-strain behavior a waiting time of two weeks was chosen between the preceding deformation and the stress relaxation experiment. Every kind of predeformation was applied to five samples. In addition, the "peak" treatment was carried out with two further specimens because of the broad scattering of the time-to-break and the achieved maximal stresses.

The reduction of the normalized stress differences in comparison to the results of stress relaxation experiments without predeformation (see Fig. 10) may suggest, that the preceding deformations had an effect on the stress. The maximal stress at the

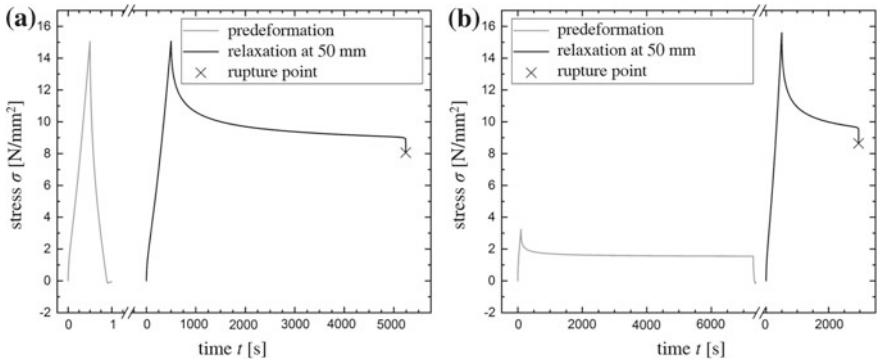

Fig. 9 Stress relaxation experiments with a preceding deformation in terms of (**a**) a 50 mm "peak", (**b**) a stress relaxation at 10 mm machine displacement

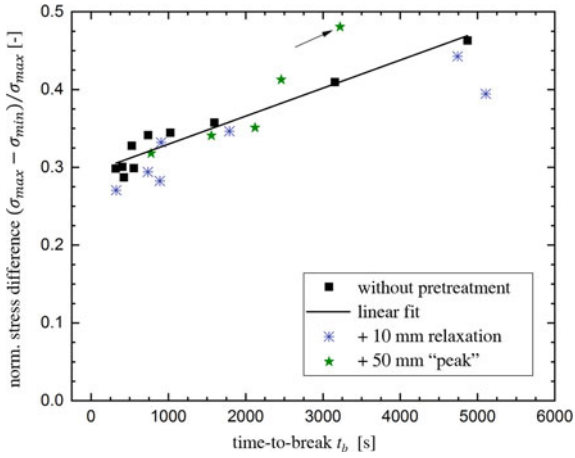

Fig. 10 Normalized stress differences of stress relaxation experiments to rupture with a preceding deformation compared to ten conventional stress relaxation experiments without pretreatment

beginning of the relaxation period was mostly less than that in conventional relaxation experiments without predeformation, whereas the time-to-break remained similar. But the slippage of pretreated samples in stress relaxation experiments was higher than that of specimen without predeformation. Consequently, the difference between the highest and the lowest maximal stress of the stress relaxation experiments with preceding treatment is two to four times higher than in the experiments without predeformation. So, the influence of a decreasing maximal stress on the initial stress decay in the relaxation period was more pronounced and caused a decrease in the normalized stress difference. Thus, this effect superposes the influence of the predeformation on stress. An arrow in Fig. 10 marks the breaking point of a specimen with a maximal stress far less compared to the other samples.

In conclusion, it is not clear, how the different kinds of preceding deformation affect the relaxation behavior and the fracture process. However, these are adequate methods to investigate the time- and strain-dependency of the damage evolution

Table 1 Testing conditions of tensile experiments to rupture (rupture points see black crosses in Fig. 11) to create a failure envelope

T [°C]	25	30	30	30	30	40	40	40	40	40
$\dot{u}$[mm/s]	0.05	0.05	0.1	0.5	10	0.02	0.05	0.1	0.5	1

provided the disturbing effect of slippage is eliminated. This can be realized by choosing a fix stress value for the beginning of the relaxation period, instead of a fix machine displacement value, in combination with DIC.

2.2.4 Failure Envelope

To test the applicability of the previously explained method of Smith and Stedry [7] to the investigated PU90/10, ten tensile tests under different testing conditions (different temperatures and constant machine rates, see Table 1) to rupture were conducted. For the sake of simplicity, tests were carried out without DIC in this preliminary study. Therefore, the measured load-at-break F_b and the achieved displacement were recorded and plotted as crosses on a load-displacement-diagram (see Fig. 11). In contrast to the method of Smith and Stedry [7], in this investigation the influence of temperature on the elastic retractive force was neglected, because the chosen temperature range was small. Hence, the load-at-break F_b is not multiplied by the ratio of a reference temperature to the testing temperature. The resulting failure envelope is estimated and sketched in Fig. 11 as a dashed line. The data of the tensile test at 40 °C and with a machine rate of 0.02 mm/s represents approximately the equilibrium curve. Three of the ten conventional stress relaxation experiments at a maximal machine displacement of 50 mm to rupture and the previously mentioned stress relaxation experiment at 10 mm over 18 h without failure are also displayed in the diagram.

Remarkably, the three samples, that relaxed at 50 mm, did not break until the decreasing load intersected the failure envelope during the relaxation period. However, in the relaxation test at 10 mm the load reached the equilibrium curve and the sample did not break even after 18 h. Therefore, the experiments show the material behavior, that was expected by the theory of Smith and Stedry [7]. The failure envelope appears to be an adequate possibility of estimating the stress-at-break σ_b (here: the load-at-break F_b) in a stress relaxation experiment and a prediction of the time-to-break can be possible, provided that the relaxation rate is known.

3 Discussion

Of course, the interpretation of the shown results should be handled with care. The fracture process and the time-to-break is subjected to significant statistical fluctua-

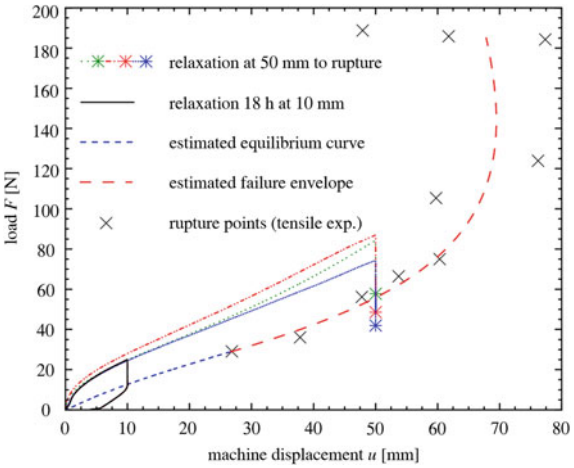

Fig. 11 Rupture points measured in tensile experiments build a failure envelope, which is compared to three conventional stress relaxation experiments to rupture (maximal machine displacement of 50 mm) and one conventional stress relaxation experiment without rupture (18 h at a maximal machine displacement of 10 mm)

tions. Hence, the small number of experiments just allows to observe tendencies. In further investigations the conclusions have to be verified by a larger number of samples per experiment. Besides, the storage of the specimen was humidity controlled but during testing it was not possible to adjust the humidity. So, it is not clear how moisture absorption influences the results.

Further tests should be carried out with optimized clamps, combined with DIC and a modification of the discontinuous relaxation experiments without waiting time. To modify the interrupted experiments, the first cycle can be conducted as shown in the present investigation. But afterwards, the maximal stress achieved in the first cycle determines the beginning of the stress relaxation period in all further cycles in order to reduce the influence of slippage of the samples out of the clamps on the maximal stress. Therefore, the initial stress decay in the relaxation period will be less dependent on slippage. In general, this modification is applicable, because it turned out that the stress-strain behavior is not considerably influenced by slippage. The suggested modification reduces the effect of the viscoelastic properties on the results of experiments without waiting time. These results will be more comparable to those of experiments with waiting time. Consequently, these tests will show, if there are recovery phenomena during unloading and in the unloaded state, that reduce or at least retard damage. Furthermore, it will be possible to study the effect of the predeformation on stress and therefore on damage evolution and on the time-to-break. Relaxation experiments with a foregoing relaxation at 10 mm machine displacement over two hours then will provide information about the appearance of damage at low strains.

In cyclic experiments, samples broke after a certain number of cycles. Combined with the conclusion that damage is not only influenced by the overall time at high strains, but also by the loading history, the question arises, whether damage processes already proceed during loading and unloading, but need some time to fully develop. A preceding deformation in form of one single cycle together with the above explained modification of the experiments will clarify, if damage processes need enough time to form by causing the samples to fail earlier.

In Sect. 2.2.4 the applicability of the method of Smith and Stedry [7] to the investigated PU90/10 is analyzed. Similar to the results of Friedrich [6] there is a lower threshold strain value, which is dependent on temperature and strain rate. This threshold defines a low strain range within which samples do not break in a relaxation experiment. In addition, in Friedrich [6] damage became minimal at an intermediate machine rate. Equally, in the investigations of Smith [12] the strain-at-break reached a maximum at a certain strain rate, so the damage became less. In this preliminary study, it appears to be possible to estimate the stress-at-break σ_b in stress relaxation with the failure envelope. This has to be verified in further investigations combined with DIC to allow the calculation of $\log(\sigma_b\ T_R/T)$ and $\log(\varepsilon_b)$ and to create a diagram similar to that of Smith and Stedry [7]. Besides, more tensile experiments to rupture have to be conducted to improve the approximation of the failure envelope. Also the capability of the method should be proved with a number of different relaxation experiments at different machine rates, temperatures and maximal machine displacements.

4 Conclusion

In spite of the small number of repetition per experiment, the results show the potential of the presented methods for analyzing the damage behavior of the investigated polyurethane. Discontinuous stress relaxation experiments led to the conclusion, that damage not only depends on the overall time at high strains, but is also influenced by the loading history. Cyclic experiments (discontinuous stress relaxation experiments without waiting time and holding time) proved, that damage already proceeds during loading and unloading. However, it should be clear, that the statistical uncertainty in those findings is very large, but the results display qualitative trends.

Moreover, in a preliminary study the method of Smith and Stedry [7] appeared to be adequate to estimate the stress-at-break in a stress relaxation experiment with a given maximal stress. Provided the relaxation behavior of PU90/10 in the relaxation phase is known, the time-to-break can also be predicted. The method holds potential for the prediction of the probability of fracture during the relaxation period and the time-to-break.

Acknowledgements We gratefully acknowledge the support of Prof. Dr. rer. nat. habil. Wulff Possart, Chair for Adhesion and Interphases in Polymers, Saarland University, for providing access to materials and equipment for sample preparation and to the dry box.

References

1. Tobolsky AV (1956) Stress relaxation studies of the viscoelastic properties of polymers. J App Phys 27:673–685
2. Bergström JS, Boyce MC (1998) Constitutive modeling of the large strain time-dependent behavior of elastomers. J Mech Phys Solids 46:931–954
3. Kahn AS, Lopez-Pamies O (2002) Time and temperature dependent response and relaxation of a soft polymer. Int J Plasticity 18:1359–1372
4. Tobolsky AV, Prettyman IB, Dillon JH (1944) Stress relaxation of natural and synthetic rubber stocks. Rubber Chem Technol 17:551–575
5. Kausch HH (2012) Polymer fracture. Springer Science & Business Media, Berlin
6. Friedrich L (2017) Untersuchungen zum Materialverhalten poröser Elastomere während der Relaxation. Bachelor thesis, Chair of Applied Mechanics, Saarland University
7. Smith TL, Stedry PJ (1960) Time and temperature dependence of the ultimate properties of an SBR rubber at constant elongations. J Appl Phys 31:1892–1898
8. Smith TL (1963) Ultimate tensile properties of elastomers. I. Characterization by a time and temperature independent failure envelope. J Polym Sci Part A General Papers 1:3597–3615
9. Smith TL (1964) Ultimate tensile properties of elastomers. II. Comparison of failure envelopes for unfilled vulcanizates. Rubber Chem Technol 4:792–807
10. Lai JS, Findley WN (1968) Stress relaxation of nonlinear viscoelastic material under uniaxial strain. Trans Soc Rheol 12:259–280
11. Wang TT, Klosner JM (1969) Relaxation properties of polyester-based polyurethane under small deformations superposed on large deformations. Trans Soc Rheol 13:193–208
12. Smith TL (1958) Dependence of the ultimate properties of a GR-S rubber on strain rate and temperature. J Polym Sci 32:99–113

Identification of Inelastic Parameters of the AISI 304 Stainless Steel

Miguel Vaz Jr., E. R. Hulse and M. Tomiyama

Abstract A proper choice of inelastic parameters is one of the most important aspects for a successful simulation of metal forming processes. Several issues must be observed when choosing such parameters, amongst which the compatibility between the magnitude of the plastic deformation of the target forming operation and the mechanical test employed to obtain those parameters. Within this context, the present work addresses the suitability of selected phenomenological hardening models and identification of the corresponding inelastic parameters based on curve-fitting strategies (logarithmic-based equations) and optimization methods (non-logarithmic models) for the AISI 304 austenitic stainless steel. Tensile tests were performed using specimens of different sizes. Based on a combined assessment of all types of specimens, it was observed that the curve-fitting technique was able to describe with excellent accuracy deformations up to maximum load. In order to contemplate larger plastic deformations, an inverse problem strategy based on optimization methods was used to account for material response up to macroscopic failure of the specimens. Numerical simulation of the tensile tests shows that the latter technique associated with non-logarithmic hardening equations provided the best approximation to the experimental data.

1 Introduction

Austenitic stainless steels are the most widely used type of corrosion-resistant steels. This class of steels are generally characterized by containing low levels of Carbon and high levels of Chromium and Nickel. In addition to Cr and Ni, other elements

M. Vaz Jr. (✉) · E. R. Hulse · M. Tomiyama
State University of Santa Catarina, Campus Universitário Prof. Avelino Marcante, Joinville 89219-710, Brazil
e-mail: Miguel.Vaz@udesc.br

E. R. Hulse
e-mail: emilio.r.hulse@embraco.com

M. Tomiyama
e-mail: masahiro.tomiyama@udesc.br

A. Öchsner and H. Altenbach (eds.), *Engineering Design Applications II*,
Advanced Structured Materials 113, https://doi.org/10.1007/978-3-030-20801-1_2

may be added in order to confer specific properties and characteristics to the material, e.g. Molybdenum to increase pitting resistance, Phosphorus and Sulphur to improve machinability, Selenium for better machined surfaces, Boron to enhance the steel capacity to absorb neutrons in nuclear thermal reactors, Silicon for higher heat resistance and Copper to improve cold working, amongst other elements [1]. The stainless steel AISI 304 is the most used grade due to its combination of mechanical (formability and weldability) and chemical (corrosion and oxidation resistance) characteristics.

The good formability of the type 304 stainless steel is associated with its relatively low yield stress and high ductility, thereby allowing large plastic deformation before onset of mechanical failure. Such features favour cold working processing [2] (roll forming, deep drawing, etc.), making possible to manufacture with greater efficiency a wide range of products and components, including consumer items, architectural elements and industrial equipment. Therefore, a proper description of mechanical properties is highly significant to industries, especially when using computational packages to simulate metal forming operations (the user must provide actual inelastic parameters). This work is inserted in this context, aiming to contribute to the discussion by assessing the suitability of some selected phenomenological equations to model hardening evolution and alternative strategies to obtain the corresponding parameters.

Form the viewpoint of tool design and prediction of manufacturing costs, including the modern concept of energy accountability, the issues briefly discussed in the previous paragraph highlights the necessity to develop a methodology to determine material parameters. Material parameters describe different aspects of the nature of the material, ranging from mechanical and thermal behaviour to chemical kinetics. The strategy addressed in this work is primarily concerned with mechanical parameters in association with inelastic deformation.

The literature shows an increasing number of works discussing strategies to determine different types of inelastic parameters, which in turn are associated with the material constitutive relation (plastic, viscoplastic, etc.) and purpose of the analysis itself (hardening, damage, etc.). Techniques based on *curve fitting* and *optimization methods* have been largely adopted in this class of problems. For instance, the suitability of selected hardening equations to describe plastic deformation of ductile materials was addressed by Samuel and co-workers [3, 4]. The authors studied several ductile materials, amongst which the AISI 316L stainless steel, and used a *curve-fitting technique* up to instability onset to obtain the hardening parameters. One of the relevant works on the application of *optimization methods* to obtain hardening parameters was presented by Ponthot and Kleinermann [5]. The study is mostly focused on mathematical aspects of several gradient-based optimization schemes. The authors proposed application in cascade of optimization methods to identification of hardening parameters of the ASTM A533, Grade B, Class 1 low alloy steel based on tensile tests.

A discussion on the hardening behaviour and a proposal of a new phenomenological hardening equation were presented by Dimatteo et al. [6] for Dual Phase (DP) 450/600/800/1000 and Transformation Induced Plasticity (TRIP) 800 steels.

A *curve-fitting strategy* associated with tensile tests was adopted to determine the hardening parameters of a new 3rd order logarithmic yield stress curve. The validation procedure indicated excellent correlation of the engineering stress and strain curves up to maximum load. Noticeably, the present work also investigates the suitability of the hardening equation proposed by Dimatteo et al. [6] to describe isothermal hardening evolution for the AISI 304 stainless steel. A parameter identification technique using *optimization methods* was used by Vaz Jr. et al. [7] to obtain hardening and fracture parameters of low Carbon AISI 1020 steel. The authors discussed application of hybrid optimization strategies and described an experimental-numerical scheme to determine inelastic parameters for two damage constitutive relations.

The brief review presented in the previous paragraphs is not exhaustive and intends to illustrate some of the existing approaches regarding the nature of the inelastic parameters and methodology of parameter identification. It is important to mention that other relevant investigations on the subject are discussed later in the appropriate sections. The present work addresses the suitability of selected phenomenological hardening models and identification of the corresponding inelastic parameters based on *curve-fitting strategies* (logarithmic-based equations) and *optimization methods* (non-logarithmic models) for the AISI 304 stainless steel. The chapter is organized as follows: Section 2 introduces a discussion on logarithmic-based phenomenological hardening equations and its intrinsic association with curve-fitting procedures. Section 3 presents alternative, non-logarithmic hardening equations and an optimization-based strategy to obtain the corresponding hardening parameters. Application of both parameter identification techniques is discussed in Sect. 4 based on tensile tests using specimens of different sizes prepared according to two different technical standards. The main conclusions and remarks are summarised in Sect. 5.

2 Phenomenological Hardening Equations and Curve Fitting Strategies

Tensile tests associated with curve fitting strategies have largely been adopted to determine yield stress parameters for metal materials. In addition to its simplicity, this technique makes possible to directly correlate *true stresses* and *true strains*, thereby conferring a straightforward physical significance. For the sake of objectivity, the reader is referred to Davis [8] for a detailed description of the method, including experimental considerations and requirements. Notwithstanding, it is relevant to emphasise that logarithmic true strains and true stresses represent the actual state of the material and are derived by considering the actual area and length of the specimen as well as constant volume during plastic deformation. The assumption of uniform deformation required by this method restricts evaluation of strains and stresses up to necking (instability) onset. The curve fitting technique is particularly significant when determining the material parameters based on specimens of different sizes. This strategy evinces eventual measurement discrepancies: in spite of different

levels of tensile loads (owing to different cross-sectional areas), the true stress strain curves for each test must show very close approximation up to maximum load.

The literature shows a wide range of empirical equations to describe the yield stress based on logarithmic, $(\ln\sigma) \times (\ln\varepsilon)$ curves. This work addresses yield stress described by the classical Swift's equation [9] and alternative approaches, such as the double-n Swift [10] and a third-order logarithmic polynomial curve [6] (referred here also as cubic logarithmic equation).

One of the most well-known yield stress equation is due to Swift [9]. The author addressed mathematically the conditions for instability of plastic strains based on the Mises-Henky constitutive model. The instability conditions were demonstrated for a strain-hardening material described by the empirical relation

$$\sigma_Y = k\left(\bar{\varepsilon}_p + \varepsilon_0\right)^n, \tag{1}$$

where σ_Y is the yield stress, $\bar{\varepsilon}_p$ is the equivalent plastic strain, k is known as strength coefficient, n is the strain-hardening exponent, and ε_0 is an initial measure of the plastic state of the material (referred here as initial strain). The fitting constants k and n can be easily determined from double logarithm plot of the experimental true stress-strain data within the envelope comprised by the elastic deformation and onset of plastic instability (maximum load). The initial strain, ε_0, is obtained by the intersection of the uniaxial elastic and plastic curves, $\sigma_0 = E\varepsilon_0 = k\varepsilon_0^n$, so that $\varepsilon_0 = (E/k)^{1/(n-1)}$, where σ_0 is the initial yield stress and E is the Young's modulus.

Further modifications of Eq. (1) have been proposed to accommodate non-linear variations of the hardening evolution. Hertelé et al. [10] highlight the fact that two-stage hardening has been observed in various types of metals, including stainless steels. The authors proposed a strategy based on the Ramberg-Osgood equation and presented results for the DIN 1.4462 duplex stainless steel. Kashyap et al. [11, 12] adopted two and three stages of the Holloman relation, $\sigma_Y = k\varepsilon^n$, to describe the behaviour of the AISI 316L stainless steel under high temperature.

In the present work, a double-n Swift curve is investigated, so that

$$\sigma_Y = \begin{cases} k_1(\bar{\varepsilon}_p + \varepsilon_0)^{n_1} & \text{if} \quad \bar{\varepsilon}_p \leqslant \bar{\varepsilon}_p^T \\ k_2(\bar{\varepsilon}_p + \varepsilon_0)^{n_2} & \text{if} \quad \bar{\varepsilon}_p > \bar{\varepsilon}_p^T \end{cases}, \tag{2}$$

in which k_1 and k_2 are the strength coefficients of each stage, n_1 and n_2 are the corresponding hardening indices, $\varepsilon_0 = (E/k_1)^{1/(n_1-1)}$ is the initial strain, and $\varepsilon_p^T = \varepsilon^T - \varepsilon_0 = \exp[\ln(k_1/k_2)/(n_2 - n_1)] - \varepsilon_0$ is the transitional equivalent plastic strain.

The material parameters (k_1, n_1) and (k_2, n_2) of Eq. (2) can be obtained from a double logarithmic plot of the experimental true stress-true strain data based on the assumption of uniform plastic deformation. The key aspect of the double-n Swift curve is the proper computation of the transition point. In this work, the transition between curves "1" and "2" is determined by minimizing a combination of the fitting errors of both hardening stages when determining parameters (k_1, n_1) and (k_2, n_2) (the technique makes use of a simple line search method which maximizes

the average coefficient of determination, $\overline{R}^2(\varepsilon^T) = (R_1^2 + R_2^2)/2$, of curves "1" and "2"). It is also important to note that, contrasting to other empirical equations, the material parameters k and n of the Swift and double-n Swift curves provide a strong physical and technological significance. The strength coefficient, k, directly indicates the magnitude of the forces involved in forming operations, whereas the value of the hardening exponent, n, points out preferred forming processes according to its level.

Within the framework of empirical descriptions of plastic deformation, Dimatteo et al. [6] proposed use of a 3rd order $(\ln\sigma) \times (\ln\varepsilon)$ polynomial fit to DP and TRIP steels in an attempt to predict the influence of alloying elements and heat treatment conditions in a simple manner. This work investigates a possible extension of the applicability range to the AISI 304 stainless steel. In the present study, provision for the elastic envelope is also included, so that

$$\ln(\sigma_Y) = A[\ln(\bar{\varepsilon}_p + \varepsilon_0)]^3 + B[\ln(\bar{\varepsilon}_p + \varepsilon_0)]^2 + C[\ln(\bar{\varepsilon}_p + \varepsilon_0)] + D, \tag{3}$$

where A, B, C, and D are the model parameters to be determined by the curve fitting procedure. Similarly to Swift's equation, the initial strain, ε_0, is obtained by the intersection between the uniaxial elastic and plastic curves and solving the cubic equation, $A[\ln(\varepsilon_0)]^3 + B[\ln(\varepsilon_0)]^2 + (C-1)[\ln(\varepsilon_0)] + [D - \ln(E)] = 0$, for the initial strain.
Remark (i): The curve fitting procedures seek the best approximation under uniaxial stress conditions. Therefore, a combination of such strategy and the aforementioned hardening equations does not guarantee a priori accurate yield stress predictions beyond the instability point. This fact has important implications when computing the actual forming load for large plastic deformations, as discussed in the following sections.
Remark (ii): It is relevant to mention that the AISI 304 stainless steel is subject to deformation-induced phase transformation of austenite to martensite. The phase transformation mechanisms give rise to complex hardening behaviour according temperature and strain rates. De et al. [13] indicate that the stress-strain curves for low strain rates and temperatures higher than 298 K follow a typical "parabolic" evolution, which, therefore, makes possible to model inelastic deformation using straightforward phenomenological approaches.

3 Alternative Yield Stress Equations and Identification of Material Parameters

It is particularly relevant to acknowledge that phenomenological constitutive models have been largely used (and preferred) in industry. Moreover, many non-logarithmic hardening equations are empirical in nature and have been recommended for individual materials or else portraying specific internal structures (see, for instance, Larour [14] and references therein). However, there have been proposed some yield stress equations derived by using micromechanical concepts that can also be applied within